applied sciences

MDPI

Article

Evaluation of the Potential for Estimating Backscattering Coefficients over Bare Agricultural Soils at the Intra-Plot Scale

Remy Fieuzal [1,*] and Frédéric Baup [1,2]

[1] Centre d'Études Spatiales de la BIOsphère (CESBIO), Université de Toulouse, CNES/CNRS/INRAE/IRD/UT3, 18 Avenue Edouard Belin, 31401 Toulouse, France; frederic.baup@univ-tlse3.fr
[2] IUT Paul Sabatier, 24 rue d'Embaquès, 32000 Auch, France
* Correspondence: remy.fieuzal@univ-tlse3.fr; Tel.: +33-561556484

Abstract: The objective of this study is to model backscattering coefficients over bare soils at intra-plot spatial scales (from almost 80 to 2800 m^2), in a context where the plot is the reference spatial scale in most past studies. A statistical modeling approach, based on a random forest algorithm, is proposed to overcome the limits of semi-empirical or physical models pointed out in the literature and to reduce discrepancies observed between the satellite-derived backscattering coefficients and the predicted values. The experimental device was set up on a network of agricultural plots located in southwestern France during the Multispectral Crop Monitoring (MCM) experiment. The dataset combines high spatial resolution satellite images (acquired by TerraSAR-X and Radarsat-2) together with synchronous geo-located measurements of key soil parameters (i.e., top soil moisture, surface roughness, and soil texture) on consistent spatial areas. Backscattering coefficients are estimated at six intra-plot spatial scales (from ~80 to ~2800 m^2), showing an exponential increase in modeling performance, and reaching higher levels of accuracy than previous work performed at the plot spatial scale (i.e., 50% of variance explained in the literature, in the best cases). The increase in signal quality with the spatial scale mainly explains the higher performance observed in the 2800 m^2 area, with a correlation of 0.91 and RMSE of 0.83 dB in the X-band (for backscattering coefficients acquired with the HH polarization state). In the C-band, the values of correlation range from 0.74 to 0.80, and the RMSE from 1.65 to 1.85 dB (depending on the considered polarization state). The results also showed that the developed statistical algorithm is mainly influenced by the surface roughness and the top soil moisture, as semi-empirical or physical-based models. Soil texture does not significantly affect the algorithm.

Keywords: backscattering coefficient modeling; bare soil; intra-plot spatial scale; Radarsat-2; random forest; TerraSAR-X

check for updates

Academic Editor: Mauro Lo Brutto

Received: 31 December 2024
Revised: 7 February 2025
Accepted: 10 February 2025
Published: 11 February 2025

Citation: Fieuzal, R.; Baup, F. Evaluation of the Potential for Estimating Backscattering Coefficients over Bare Agricultural Soils at the Intra-Plot Scale. *Appl. Sci.* **2025**, *15*, 1827. https://doi.org/10.3390/app15041827

Copyright: © 2025 by the authors. Licensee MDPI, Basel, Switzerland. This article is an open access article distributed under the terms and conditions of the Creative Commons Attribution (CC BY) license (https://creativecommons.org/licenses/by/4.0/).

1. Introduction

Several studies have established performance levels and discussed the limitations and main biases of the most commonly used backscatter models for estimating microwave signals over bare soils [1–7]. Initially, the studies carried out on study sites with a wide range of surface conditions were used to qualify the performance levels of various electromagnetic models. Semi-empirical approaches, as proposed by Oh et al. and Dubois et al. [8–10], as well as physically based models, such as the IEM [11–13], were implemented, and estimates of backscattering coefficients were compared with the values derived from satellite images. In those works, the best performance levels were associated with semi-empirical models, with error levels varying between 2.3 and 4.7 dB, and higher

correlations in the X-band (with values close to 0.60) compared with those observed in the C-band (values below 0.50). Those previous studies have highlighted the limitations of existing models, and identified which variables were poorly taken into account in the original approaches. Correcting these biases then became a major focus of work on electromagnetic modeling. Various modalities were then proposed, with an emphasis on roughness descriptors (each of the studies presenting a modification of the formalism with respect to this variable), resulting in new versions of the models. In the end, this work made it possible to extend the validity of backscatter models, notably to the wide range of roughness levels observable in agricultural conditions. However, there is no consensus on any of the proposed models, whatever the considered assumption regarding formalism, as they still have important limitations (with an explained variance level close to 50%, in the best cases [5]). The difficulty in obtaining higher levels of performance is partly explained by the spatial scale at which these studies were conducted. In those studies, satellite signals and ground measurements were aggregated/averaged at the scale of the agricultural plot, an entity that can show strong contrasts in soil conditions. This variability within the plot may be highlighted by a difference in backscatter levels closely related to moisture [14], texture [15], or roughness [16], and delimiting intra-plot spatial patterns with comparable values.

With access to high spatial resolution SAR images which are becoming more systematic with current and future satellite missions (Sentinel-1, Radarsat constellation, TerraSAR-X, Tandem-X...), one challenge is to use these images at a resolution close to the pixel, while limiting speckle effects [17]. Deriving metrics of interest on an intra-plot scale is a major challenge, particularly in the context of precision agriculture, where modulation approaches based on satellite images mainly use optical data [18,19]. Integrating SAR signals into these methods would provide information that could replace optical data (in the case of unfavorable atmospheric conditions) or complement it (when the signals provide differentiated information), as shown by work carried out in vegetative periods [20,21]. Moreover, the definition of this spatial scale would be particularly useful for studies aimed at estimating surface humidity at very high resolution, as the statistical performances associated with current approaches are limited and contrasted [22].

In this context, this study aims at evaluating the possibilities of estimating backscattering coefficients in X- and C-bands, on bare soils at the intra-plot spatial scale, using the random forest (RF) algorithm [23]. Such a statistical approach has already been implemented at the spatial scale of the plot [24], showing a significant increase in accuracy compared to semi-empirical (proposed by Oh et al. and Dubois et al. [8–10]) or physical models (IEM [11–13]) as well as to modified models involving a change in the formalism to correct observed biases [5,6].

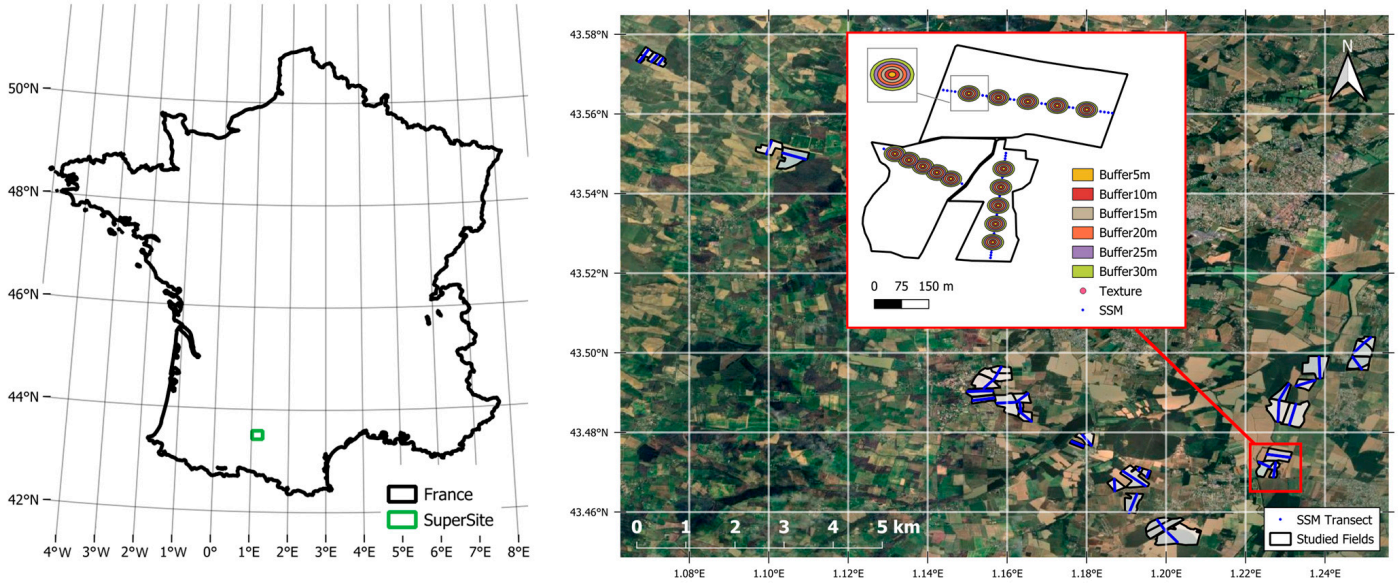
The article is structured as follows: The study site and the data collected in the plots (surface soil moisture, texture, and roughness) are presented first, along with the main characteristics of the TerraSAR-X and Radarsat-2 images (Section 2.1). The steps involved in estimating SAR signals at several intra-parcel spatial scales are then described (Section 2.2). The results section deals first with the performance obtained in the X-band, then in the C-band (Section 3). The discussion (Section 4) is divided into two parts, dealing with SAR signal quality and the influence of input descriptors on the statistical algorithm.

2. Materials and Methods

2.1. Study Area

The study area, identified as a super site in Figure 1a, was located in southwestern France, near Toulouse (coordinates for the center of the area are 43°29′36″ N, 01°14′14″ E). The super site was part of a French observatory called Regional Spatial Observatory

South-West (RSO SW). The research activities mainly focused on monitoring and assessing natural and anthropogenic determinants of ecosystem functioning at a regional watershed scale and its landscape. The observatory was also part of the Pyrenees Garonne Regional Workshop Area (ZA PYGAR [25]) and the national Research Infrastructure Critical Zone Observatories: Research and Applications (OZCAR) [26].



(**a**) (**b**)

Figure 1. Location of the study site in southwestern France (super site in green in (**a**)), together with the network of the studied plots (37) superimposed on an ortho-image provided by the IGN (French National Geographic Institute) (**b**). An example of the experimental device is described on a zoomed window, showing the transect of surface soil moisture and texture measurements. The six considered circular buffers (5, 10, 15, 20, 25, and 30 m of radius) used to extract the satellite signal are displayed for three plots according to texture measurements.

The region was governed by a temperate climate with Mediterranean influences, with an annual rainfall of approximately 600 mm and mean daily air temperature ranging from a few degrees in winter to 25 °C in summer. Topographical conditions were contrasted between the relatively flat eastern part (with slopes of less than 1°) and the western part, where the average slope was close to 4.5°. Agricultural soils were quite heterogeneous, with the clay, silt, and sand contents, respectively, ranging from 9% to 58%, from 22% to 77%, and from 4% to 53%. These soils fall into three classes of the European Soil Map (HYPRES) texture classification system (i.e., Fine, Medium, and Medium Fine). The study area was mainly dedicated to agricultural activities. More than half of the landscape was given over to seasonal crops (i.e., straw cereals, sunflower, maize, rapeseed, sorghum, or soybean).

2.2. Materials

During the experimental campaign carried out from February to November 2010, a network of plots with alternating vegetative periods and bare soil conditions was monitored (Figure 1b). The bare soil conditions, the main focus of the present paper, were observed after the harvest and before the sowing of the next crop (i.e., mainly in spring and autumn, Figure 2). Depending on the crop and the agricultural practices used, the number and depth of tillage methods vary between the monitored plots, resulting in contrasting roughness levels (ranging from smooth before the crop sowing to very rough after deep ploughing).

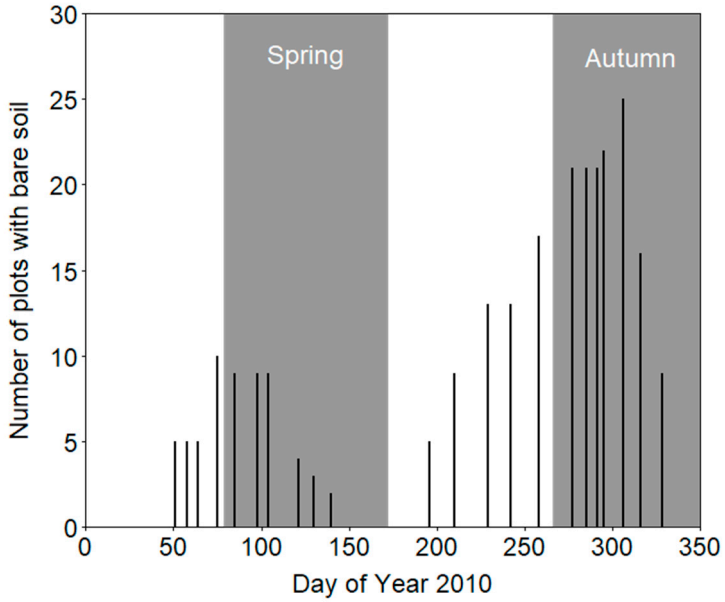


Figure 2. Temporal evolution of the number of plots (among the 37 monitored plots) with bare soil during the 2010 cropping year.

2.2.1. Ground Measurements

An overview of the collection of ground measurements is given below. The experimental set-up and protocols used to regular top soil moisture (TSM, 0–5 cm), texture, and roughness data were described in detail in [27].

On each monitored plot, transects were determined to collect geo-located measurements of TSM and texture (Figure 1). A portable ThetaProbe (ML2x) was used to collect regular measurements of TSM. By using the calibration relationship established by [27], the signal delivered in mV was converted in volumetric moisture. For texture, 2 to 8 points were geo-located on each plot. For each point, 16 cores within a 15 m diameter circle were collected (to a depth of 25 cm). Clay, silt, and sand fractions were finally derived based on element size. Measurements of the surface roughness were performed after each tillage event. Two profiles were recorded parallel and perpendicular to the direction of the tillage of the plot, using a 2 m long needle profilometer (composed of 201 needles spaced one centimeter apart). The root mean square height (hrms) and the correlation length (lc) were derived from the couple of profiles.

The ground measurements were collected quasi-synchronously with satellite acquisitions ($\Delta t < 1$ day for most measurements) on bare soils showing a wide range of surface conditions, characterized by values of TSM ranging from 3.2 to 34.9%, content in clay from 9 to 58%, hrms from 0.5 to 6.9 cm, and lc from 1.1 to 16.5 cm.

2.2.2. Microwave Satellite Images

A series of microwave satellite images were acquired by TerraSAR-X (29 images, $\lambda = 3.1$ cm). X-band data were delivered at a HH polarization state using two beam modes (Stripmap (SM) and Spotlight (SL)), with an incidence angle ranging from 27.3 to 53.3° and pixel spacing ranging from 1.5 to 3 m [28]. The main features of the TerraSAR-X images are shown in Table 1.

C-band data were delivered at a full quad-polarization (FQP) state (HH, VV, HV, and VH) by Radarsat-2 (22 images, $\lambda = 5.5$ cm). The angle of incidence varied from 24° to 41° and the pixel spacing was around 5 m [29]. The dates of each acquisition, together with details of the image configurations, are given in Table 2.

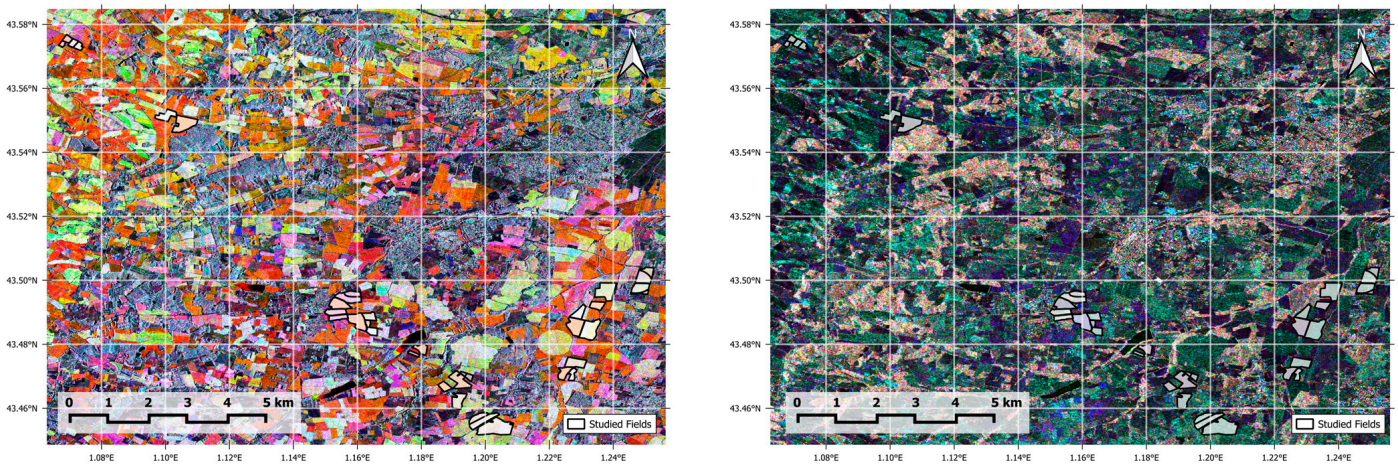
Table 1. Characteristics of satellite images acquired by TerraSAR-X in 2010.

Mode	Pass	Incidence Angle (°)	Pixel Size (°)	Acquisition Date (MM/DD)
Spotlight	D	28.7	2	03/15
Spotlight	A	32.3	2	04/14
Spotlight	A	45.5	1.75	04/08; 04/30; 08/29
Spotlight	D	53.3	1.5	03/05; 05/21; 07/15; 08/17 09/30; 10/11; 10/22 11/02; 11/13; 11/24
Stripmap	D	27.3	2.75	02/21; 03/26; 05/09; 05/20 07/14; 08/16; 09/29; 10/10 10/21; 11/12; 11/23
Stripmap	A	31.8	2.75	09/15
Stripmap	D	41.7	3	02/27; 07/31

Table 2. Characteristics of satellite images acquired by Radarsat-2 in 2010.

Mode	Pass	Incidence Angle (°)	Pixel Size (°)	Acquisition Date (MM/DD)
FQP5	A	23.3–25.3	4.7 × 4.9	03/05; 11/24
FQP6	D	24.6–26.5	4.7 × 4.7	10/21; 11/14
FQP10	A	29.1–30.9	4.7 × 5.1	02/26; 04/15; 05/09; 09/30
FQP11	D	30.2–32.0	4.7 × 5.5	03/26; 08/17
FQP15	A	34.3–36.0	4.7 × 4.8	03/15; 04/08; 05/02; 08/30; 10/17
FQP16	D	35.4–37.0	4.7 × 5.1	05/20; 07/31; 10/11
FQP20	A	39.1–40.7	4.7 × 4.8	11/03
FQP21	D	40.1–41.6	4.7 × 5.1	02/20; 03/16; 07/14

SAR images were calibrated and geo-referenced using ortho-photos (with a resolution of 50 cm) provided by the French National Geographic Institute. Color compositions based on TerraSAR-X and Radarsat-2 images (Figures 3a and 3b, respectively) reveal the highly dissected structure of the study area, as well as the strong heterogeneity between plots, linked to different surface conditions (e.g., bare soil versus vegetated plots, or with different levels of surface roughness).



(**a**) (**b**)

Figure 3. Color compositions produced on the super site from three TerraSAR-X images acquired in HH polarization in Stripmap mode (R: 20 March 2010, V: 17 August 2010, B: 24 November 2010) (**a**), and from Radarsat-2 images (R: HH, V: VV, and B: HV) acquired on 15 April 2010 (**b**).

2.3. Methodology

2.3.1. Statistical Algorithm and Explanatory Variables

Among the wide range of statistical algorithms, the Random Forest (RF, [23]) approach is particularly appropriate in a multifactorial and non-linear context such as modeling backscattering coefficients. This algorithm offers the major advantage of better predictive capability, with a performance far superior to that of multiple linear regressions [24]. In addition, this algorithm has been used in the field of remote sensing, notably with microwave images, in contexts of land use and land cover classification, or for the estimation of variables of interest such as soil moisture [30,31].

A quantitative estimation of the targeted variable is obtained through a weighted mean of an ensemble of estimations. The bootstrap aggregating procedure allows constructing independent trees on a subset of samples derived from the original dataset, and presents the following advantages: a reduced over fitting, a low influence of noise on the data, and a high stability of the results.

Backscattering coefficients were statistically modeled by considering the same explanatory variables as those used for semi-empirical or physical-based models [9–13]: the angle of incidence of SAR images, the soil moisture, the clay and sand fractions, and the soil roughness (hrms and lc collected in the parallel and perpendicular directions).

2.3.2. Set Up of the Algorithm at Six Intra-Plot Spatial Scales

The geo-location of texture measurements was used to extract the SAR satellite signals by considering six buffers, with a radius ranging from 5 to 30 m (corresponding to areas from ~80 to ~2800 m^2), and to select the top soil moisture measurements performed within these areas of interest (Figure 1). Above 30 m, there is too much overlap between zones and the radar coefficients are not independent enough. One independent RF statistical algorithm was implemented for each spatial area and each satellite configuration (distinguishing frequency and polarization states). Whatever the considered case, the dataset was randomly divided into training and validation sets, each containing half of the data. The number of available points varied according to the frequency and with the considered size of the buffer, from 725 (for the 5 m buffer) to 1014 (for other buffers) in the X-band and from 593 (for the 5 m buffer) to 798 (for other buffers) in the C-band. For each considered satellite configuration and spatial scale, the statistical algorithm was calibrated and then validated on independent datasets, repeating the procedure ten times.

2.3.3. Accuracy Metrics

The comparison of the observed and estimated values of the backscattering coefficients was evaluated using two statistical criteria: the mean values of the correlation coefficient (r, Equation (1)) and the root mean square error (RMSE, Equation (2)). The performances obtained at the intra-plot spatial scale were finally compared with those previously obtained at the plot spatial scale, using the same precision metrics [1–7,24].

$$r = \frac{\mathrm{COV}(o,p)}{\sigma_o \sigma_p}, \quad (1)$$

$$RMSE = \sqrt{\frac{\sum_{i=1}^{n}(p_i - o_i)^2}{n}}, \quad (2)$$

where n is the number of observed values, o is the observed value, p is the predicted value, COV is the covariance, and σ_o and σ_p are the standard deviations of observed and predicted data, respectively.

3. Results

3.1. Multi-Incidence Estimates in X-Band

The statistical performances obtained by comparing the backscattering coefficients modeled and the values derived from the multi-incidence TerraSAR-X images for buffers ranging from 5 to 30 m are presented in Figure 4. A notable increase in accuracy is first observed when considering the three first sizes of buffer (from 5 to 15 m), highlighted by the rise in the correlation from 0.74 to 0.89, and the decrease in RMSE from 1.56 to 0.94 dB. Then, performances saturate and the gain in accuracy only slightly increases with the size of the buffer. With a correlation close or up to 0.9 and RMSE lower than 1 dB, the performances overpass the results presented in several studies, using semi-empirical or physical models, with validation being performed at the plot spatial scale [1–7]. In these studies, model performances are first established, showing limited levels of accuracy (with correlation ranging between 0.06 and 0.59 and an error of 2.3–10.6 dB). The low performances obtained at the plot scale can be explained by the fact that parameters measured locally are not fully representative of the surface state at the plot scale. Then, some studies propose modifications of the formalism to correct certain biases (particularly with respect to roughness). The proposed methodology consists of identifying and correcting the residues of the models, depending on the surface properties (roughness, moisture, texture) and/or sensor characteristics (frequency, incidence angle). They obtained an improvement in accuracy, with a correlation of 0.69 and error of 1.41 dB, for the best performance obtained with a modified version of the model proposed by Dubois [5,10].

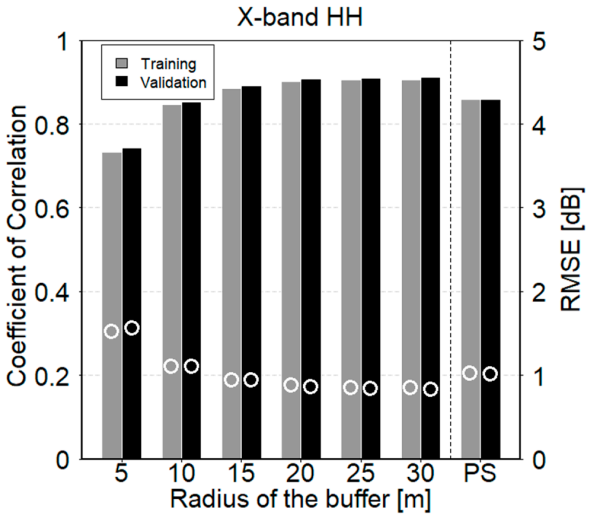


Figure 4. Evolution of the statistical performances (coefficients of correlation and root mean square errors, bars and dots, respectively) with the buffer's size and at the plot spatial scale (PS, [24]) for the training (gray) or validation (black) subsets of samples.

Figure 5 presents an example of comparison between modeled and satellite-derived backscattering coefficients for the buffer of 30 m. At this spatial scale, the proposed approach is associated with a high level of performance (during training and validation steps), as evidenced by the correlation of 0.91 (0.91) and the low RMSE of 0.85 (0.83) dB for the training and (validation), respectively. Such a level of performance exceeds the previous results obtained at the spatial scale of the plot (correlation of 0.86 and error of 1.01 dB [24]). Beyond the good overall performance, one phenomenon is particularly interesting to analyze: the overestimation of simulations for low measured values of the backscattering coefficient. These conditions apply to smooth, bare, dry soils, for which too little field data are available to train the statistical model. More measurements are needed to make up for this deficiency.

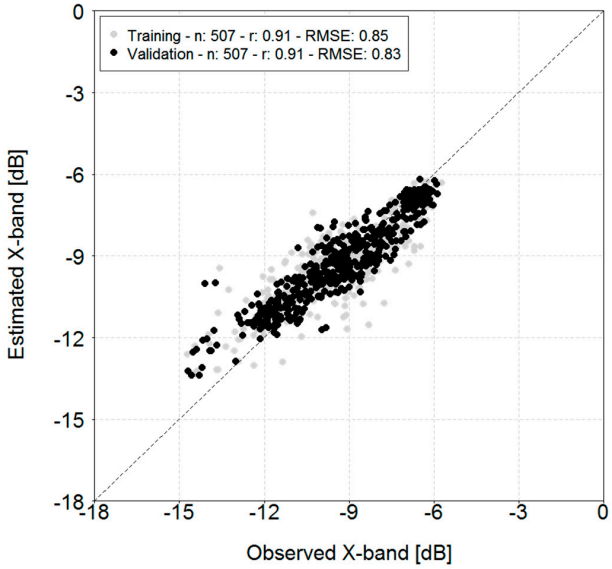


Figure 5. Comparison between simulated and observed backscattering coefficients in X-band for a buffer with a radius of 30 m. The gray or black colors represent the training or validation datasets, respectively.

3.2. Multi-Incidence and Multi-Polarization Estimates in C-Band

In the C-band, independent statistical algorithms are trained and validated by distinguishing the polarization states and, as previously conducted, for buffers ranging from 5 to 30 m (Figure 6). The evolution of statistical performance with the size of the buffer shows a similar behavior whatever the considered polarization state. A significant increase in the coefficient of correlation is observed for the first four intra-plot studied spatial scales (with correlation values increasing from 0.29 to 0.71, and a decrease in RMSE of more than 2.3 dB, on average), with the gain of accuracy being more moderate for the buffers of 25 and 30 m. In comparison with the X-band, the coefficient of correlation associated with the first spatial scale is very low in the C-band. Despite the increase in performances accompanying the change in the intra-plot spatial scale, they remain lower than those obtained previously for the X-band.

The level of accuracy obtained for the C-band is acceptable and fully consistent with past studies [1–3,5–7], where several types of modeling were evaluated and classified into two categories: physical-based [11–13,32,33] and empirical (or semi-empirical) models [6,8–10]. In the present study, for a buffer with a radius of 30 m, the values of correlation and RMSE are close for modeled co-polarized backscattering coefficients (r close to 0.75 and RMSE of 1.67 dB), while cross-polarized backscattering coefficients are estimated with higher correlation and RMSE (r of 0.80 and RMSE of 1.86 dB) values derived from the validation subset of 399 samples (Figure 7). As observed in the X-band, the values of the RMSE and correlation obtained with a buffer of 30 m (or even with a buffer of 25 m for some polarization states) are higher than those obtained with smaller buffers and at plot scale (as observed and explained for the X-band, Figure 6). The phenomenon of under sampling of surface conditions observed in the X-band is also observed in the C-band. It causes bad simulations for low and high values of the backscattering coefficient (whatever the polarization: VV, HH, and VH) due to smooth and dry or rough and wet surface conditions. As for the X-band, more ground data are requested for these conditions.

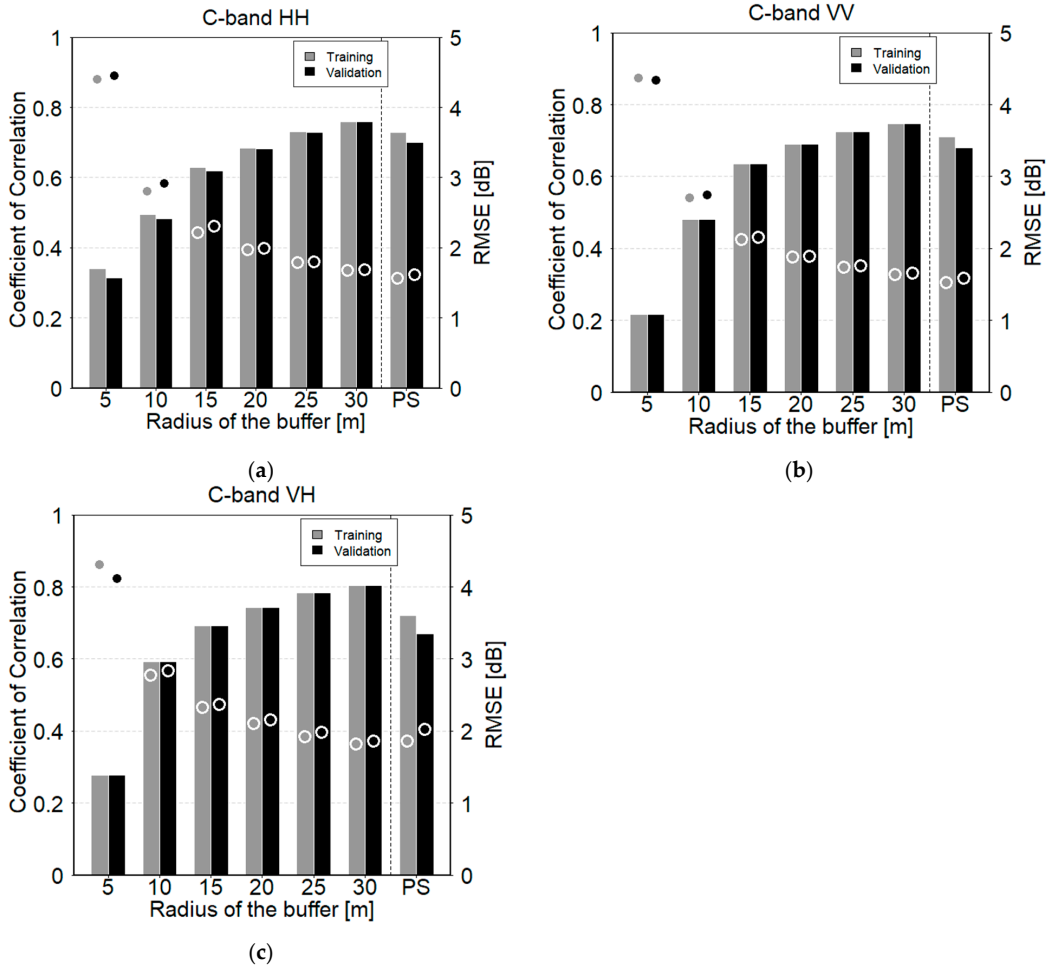


Figure 6. Evolution of the statistical performances (coefficients of correlation and root mean square errors, bars and dots, respectively) with the buffer's size and at the plot spatial scale (PS, [24]) for the training (gray) or validation (black) subsets of samples. Results obtained in C-band in three polarization states: (**a**) HH, (**b**) VV, and (**c**) VH.

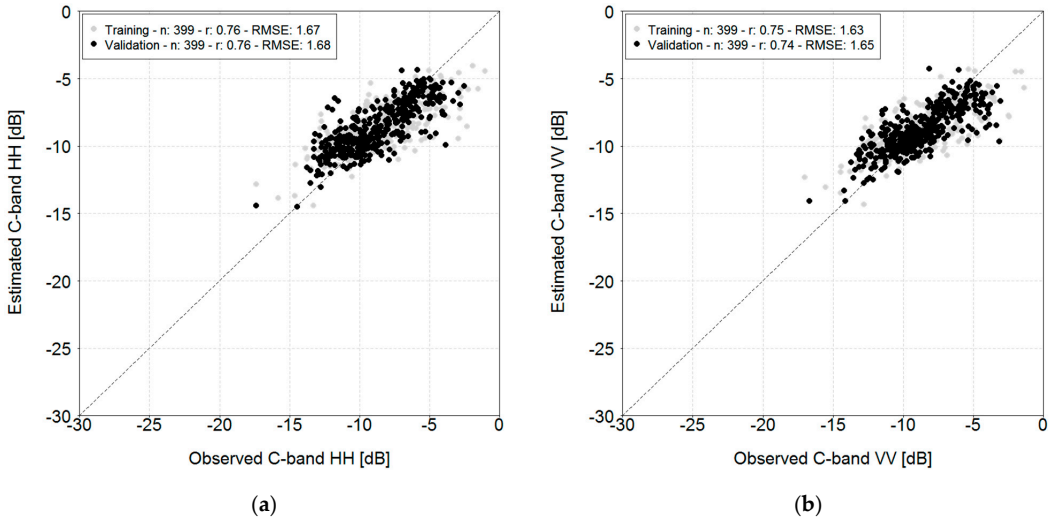
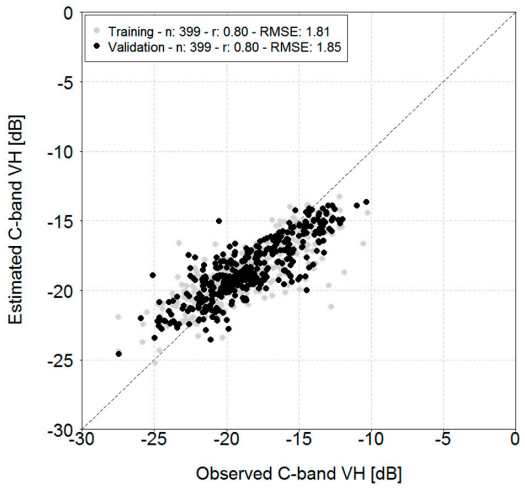


Figure 7. *Cont.*



(**c**)

Figure 7. Comparison between observed and estimated backscattering coefficients in C-band for a buffer with a radius of 30 m in three polarization states: (**a**) HH, (**b**) VV, and (**c**) VH. The gray and black dots represent the estimations performed considering the training or validation subsets of samples, respectively.

4. Discussion

4.1. Variability of the SAR Signal with the Spatial Scale

The variability of the SAR signal with the size of the considered area of interest is analyzed by focusing on the comparison between the values of the backscattering coefficients extracted with different buffer sizes. For each studied satellite configuration, Figure 8 shows the dispersion as well as two statistical parameters (determination coefficients and RMSE), taking as a reference the signals extracted with the best performances (with a 30 m radius), as demonstrated in Section 3. The signal variability decreases with the increasing size of the area of interest, regardless of the SAR signal, with a rate specific to the configuration of the considered image. In the X-band, the significant difference observed between the signals extracted with buffers of 5 and 30 m of radius is rapidly fading, as shown by the values of the determination coefficient and error obtained from the next spatial scale (R^2 of 0.92 and RMSE of 0.60 dB for a 10 m radius). This variability is higher in the C-band, where the thresholds of 0.9 for the determination coefficient and 1 dB for the RMSE are reached earlier, for areas of interest with a buffer of 20 m radius.

The difference in performance observed between the images acquired in the X- and C-bands is explained by the characteristics of the sensors onboard the TerraSAR-X and Radarsat-2 satellites. A first criterion for analyzing the quality of the SAR images is the noise equivalent sigma zero (NESZ), which measures the thermal noise of the instrument. In the X-band, the NESZ is equal to −19 dB regardless of the considered beam mode [34], while the C-band images acquired with the full quad-polarization mode present a best NESZ of -36.5 ± 3 dB [35]. Whatever the considered beam mode, the value of NESZ was always lower than the recorded backscattering coefficients. In these conditions, the median signal noise ratios (SNRs) are equal to 9.78 and 9.93 dB in the X-band, for a buffer with a radius of 5 and 30 m, respectively. In the C-band, higher values of SNR are observed, with minimal median values equal to 16.36 and 17.66 dB for a 5 m and 30 m buffer radius (for signals acquired with cross-polarized states), respectively. Even if some points are getting closer to the NESZ threshold at the finer spatial scale (especially in the C-band), the values of SNRs are important and acceptable in most cases. The second criterion is the radiometric resolution (RRAD). It determines the ability of a SAR system to distinguish different uniform regions by assuming negligibly the radar noise from the

distributed target. The RRAD is derived from several parameters of the SAR images (i.e., the number of azimuthal and range pixels, the number of azimuthal and range looks, the azimuth and ground range spatial resolutions, and the azimuth and ground range pixel spacing). Figure 9 presents the evolution of the RRAD with the size of the buffer for the three beam modes used in the present study. A comparable exponential decrease in the value of RRAD is observed, and more than 80% of the RRAD decrease is reached from the buffer of a 20 m radius. The beam modes are distinguished by their absolute value levels, closely related to image resolution. The RRAD values are thus maximum for the 5 m radius buffer, varying between 2.3 and 0.71 dB, and minimum for the 30 m radius buffer, where they are then between 0.49 and 0.13 dB, for modes FQP and SL, respectively. The decrease in the radiometric resolution partly explains the increase in the correlation coefficients obtained in Figures 4 and 6. Indeed, the signals extracted with poor radiometric resolution (high impact of speckle effects and low number of pixels used to calculate the median value of backscattering coefficients) give the worst simulation performance. Conversely, signals extracted with better radiometric resolutions offer better quality simulations.

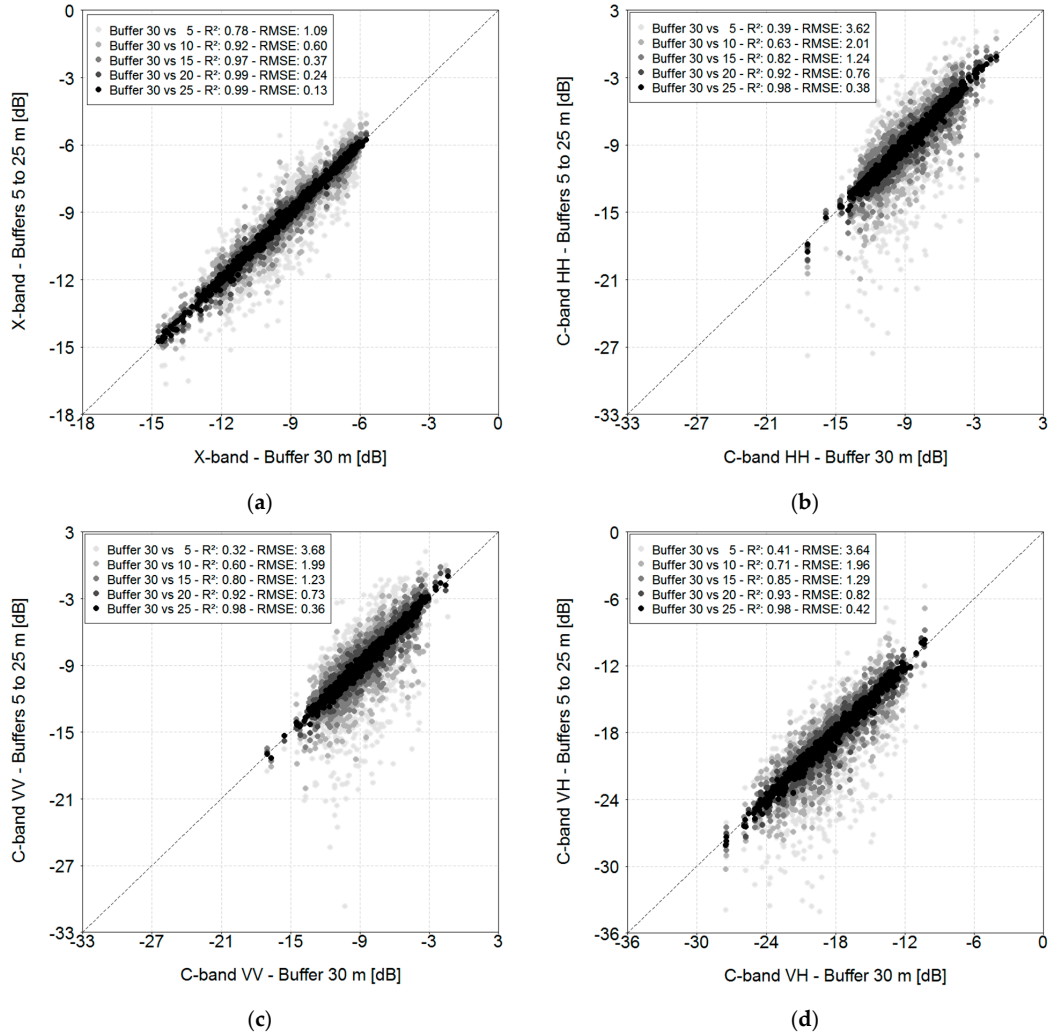


Figure 8. Comparison between the values of backscattering coefficients extracted using different sizes of buffers for the X- (**a**) and C-bands with the 3 polarization states: (**b**) HH, (**c**) VV, and (**d**) VH. Whatever the considered configuration, the buffer with a radius of 30 m is used as a reference for the comparison.

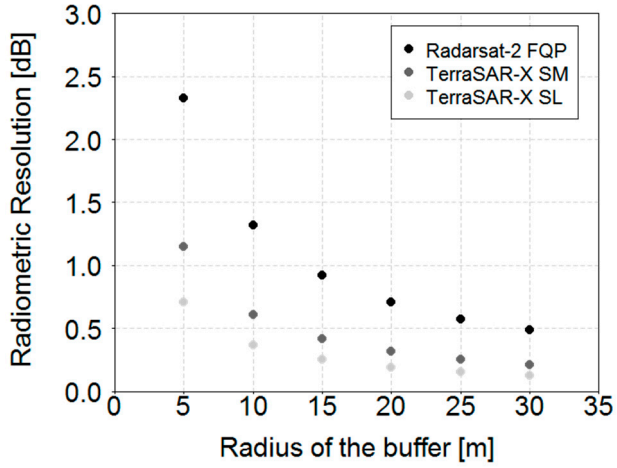


Figure 9. Evolution of the values of radiometric resolution with the buffer's size for the three studied SAR modes (full quad-polarization—FQP, Stripmap—SM, and Spotlight—SL modes).

4.2. Influence of the Explanatory Input Variables

Figure 10 summarizes the relative importance of the explanatory input variables of the modeling approach, based on the results obtained for the 30 m radius buffer. At this intra-plot spatial scale, the four components of roughness (i.e., hrms and lc measured in the perpendicular and parallel direction) have a more pronounced relative importance than other surface descriptors (TSM or texture), whatever the considered satellite configuration (with a relative importance of 31.4% in the X-band, ~37.0% and 39.3% for the co- and cross-polarization states in the C-band). Top soil moisture is the second most important variable, with 27.9% in the X-band and between 30.2 and 31.7% in the C-band (depending on the polarization state). The texture's variables only show a limited importance (reaching a maximum of 15.3% for cross-polarization states in the C-band), with the relative influence of clay content being always greater than that of the sand content.

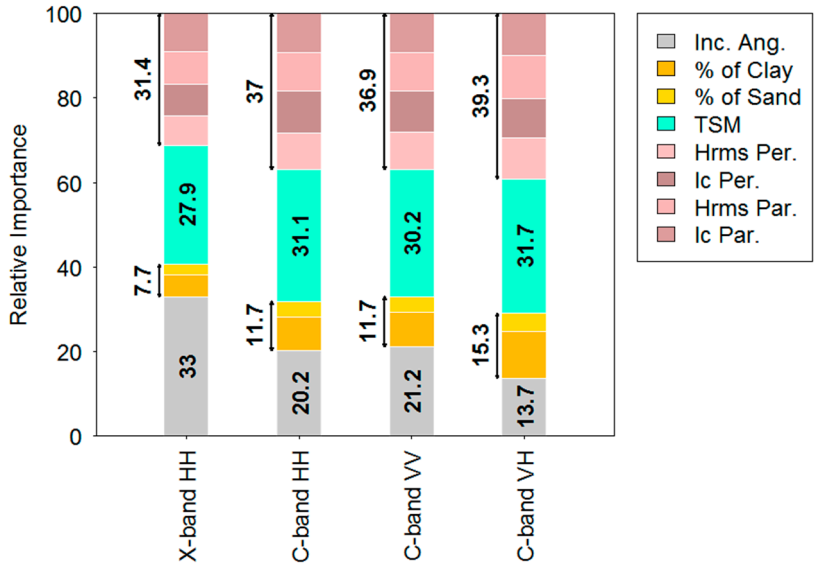


Figure 10. Relative importance of the input variables of RF algorithms for the X- and C-bands with the 3 polarization states: HH, VV, and VH, for buffer with a radius of 30 m.

These results show that the influences of the soil descriptors used in the random forest algorithm are consistent with their influences in empirical, semi-empirical, and physical-based models [6,8–13,32,33], as reflected in the higher influence of TSM and surface roughness on the estimation of backscattering coefficients, and the more limited impact

of texture. The influence of the incidence angle is minimal regarding the cross-polarized satellite signal (13.7% for VH), which is lower than the relative importance observed for co-polarized C-band signals (20.2 and 21.2% for HH and VV, respectively). Such a difference between the polarization states has been already pointed out in previous studies, showing a lower angular sensitivity of signals acquired in cross-polarization [36]. Finally, the influence of the incidence angle is higher in the X-band (reaching 33%) compared to the signals acquired with the same polarization state in the C-band (relative importance close to 20% for HH). Such difference between frequencies may be related to the range of variation of the incidence angle of the satellite images used ($\Delta\theta$ in C-band = 16°, $\Delta\theta$ in X-band = 26°).

5. Conclusions

Based on a dense dataset collected on a specific experimental device, the present study aimed at evaluating the possibilities of modeling backscattering coefficients at the intra-plot spatial scale on bare agricultural soils. The estimations of the backscattering coefficient were performed using a statistical approach, at spatial scales ranging from 80 to 2800 m^2, and compared to satellite signals acquired by TerraSAR-X and Radarsat-2. A high level of accuracy was observed in the X-band (with a correlation of 0.91 and RMSE of 0.83 dB for the 2800 m^2 area), while the explained variance was lower in the C-band (best values of correlation between 0.74 and 0.80, and RMSE between 1.65 and 1.85 dB, depending on the considered polarization state). Whatever the considered wavelength, the best performances obtained at the intra-plot spatial scale overpass the level of accuracy observed at the plot scale in the literature. By applying the modeling approach at the intra-plot scale, the spatial variability of soil surface descriptors (averaged in plot-scale approaches) is better considered. This qualification of the possibility of using radar images on an intra-plot scale opens the way to new approaches for monitoring variables of interest in an agricultural context. Nevertheless, the dataset will have to be extended with in situ measurements taken on soils with extreme conditions of roughness (smooth and very rough) and moisture (dry and saturated). In addition, the approach implemented during the bare soil period should be tested during the vegetation growing cycles. The accuracy of the intra-plot approach is strongly linked to the specificities of the microwave signals (i.e., NESZ and RRAD), which condition the possibility to get closer to the pixel size. The same approach could therefore be applied to other satellite missions (e.g., COSMO-SkyMed, TanDEM-X, Radarsat Constellation, and Sentinel-1) to study whether images can be used at different spatial scales. It could also be extended to data acquired at higher wavelengths provided by the L and P-band sensors onboard the current ALOS-2 and ALOS-4 missions, or forthcoming Biomass satellite. The performances associated with the estimation of the backscattering coefficients finally make it possible to define an area of interest specific to the considered signal (~700 m^2 and ~2000 m^2 for the tested images, respectively, acquired in the X- and C-band), useful for future approaches to estimating surface moisture or roughness at intra-plot spatial scales.

Author Contributions: Conceptualization, R.F. and F.B.; methodology, R.F. and F.B.; formal analysis, R.F. and F.B.; writing—original draft preparation, review and editing, R.F. and F.B. All authors have read and agreed to the published version of the manuscript.

Funding: This research received no external funding.

Institutional Review Board Statement: Not applicable.

Informed Consent Statement: Not applicable.

Data Availability Statement: The data presented in this study are available on request from the corresponding author.

Acknowledgments: The authors wish to thank the DLR (German Space Agency), SOAR Project and CNES (Centre National des Etudes Spatiales) for their support, funding, and satellite images (proposal HYD0611 and SOAR-EU and Categorie-1 ESA project no. 6843). In addition, the authors wish to thank the farmers (Blanquet, Bollati, Brardo, Pavan, and Peres) for their time and precious discussion and the people who helped to collect the ground data.

Conflicts of Interest: The authors declare no conflicts of interest.

References

1. Baghdadi, N.; Zribi, M. Evaluation of radar backscatter models IEM, OH and Dubois using experimental observations. *Int. J. Remote Sens.* **2006**, *27*, 3831–3852. [CrossRef]
2. Rahman, M.M.; Moran, M.S.; Thoma, D.P.; Bryant, R.; Sano, E.E.; Holifield Collins, C.D.; Skirvin, S.; Kershner, C.; Orr, B.J. A derivation of roughness correlation length for parameterizing radar backscatter models. *Int. J. Remote Sens.* **2007**, *28*, 3995–4012. [CrossRef]
3. Fieuzal, R. *Apports des Données Radar Pour L'estimation des Paramètres Biophysiques des Surfaces Agricoles*; Sciences de la Terre; Université Toulouse III-Paul Sabatier: Toulouse, France, 2013.
4. Baghdadi, N.; Saba, E.; Aubert, M.; Zribi, M.; Baup, F. Evaluation of radar backscattering models IEM, Oh, and Dubois for SAR data in X-Band over bare soils. *IEEE Geosci. Remote Sens. Lett.* **2011**, *8*, 1160–1164. [CrossRef]
5. Fieuzal, R.; Baup, F. Improvement of bare soil semiempirical radar backscattering models (Oh and Dubois) with SAR multi-spectral satellite data (at X, C and L bands). *Adv. Remote Sens.* **2016**, *5*, 296–314. [CrossRef]
6. Baghdadi, N.; Choker, M.; Zribi, M.; Hajj, M.E.; Paloscia, S.; Verhoest, N.E.C.; Lievens, H.; Baup, F.; Mattia, F. A new empirical model for radar scattering from bare soil surfaces. *Remote Sens.* **2016**, *8*, 920. [CrossRef]
7. Choker, M.; Baghdadi, N.; Zribi, M.; El Hajj, M.; Paloscia, S.; Verhoest, N.E.C.; Lievens, H.; Mattia, F. Evaluation of the Oh, Dubois and IEM backscatter models using a large dataset of SAR data and experimental soil measurements. *Water* **2017**, *9*, 38. [CrossRef]
8. Oh, Y.; Sarabandi, K.; Ulaby, F.T. An empirical model and an inversion technique for radar scattering from bare soil surfaces. *IEEE Trans. Geosci. Remote Sens.* **1992**, *30*, 370–381. [CrossRef]
9. Oh, Y. Quantitative retrieval of soil moisture content and surface roughness from multipolarized radar observations of bare soil surfaces. *IEEE Geosci. Remote Sens.* **2004**, *42*, 596–601. [CrossRef]
10. Dubois, P.C.; van Zyl, J.; Engman, T. Measuring soil moisture with imaging radars. *IEEE Trans. Geosci. Remote Sens.* **1995**, *33*, 915–926. [CrossRef]
11. Fung, A.K.; Li, Z.; Chen, K.S. Backscattering from a randomly rough dielectric surface. *IEEE Trans. Geosci. Remote Sens.* **1992**, *30*, 356–369. [CrossRef]
12. Fung, A.K. *Microwave Scattering and Emission Models and Their Applications*; Artech House Publishers: Norwood, MA, USA, 1994.
13. Chen, K.S.; Wu, T.D.; Tsay, M.K.; Fung, A.K. A note on the multiple scattering in an IEM model. *IEEE Trans. Geosci. Remote Sens.* **2000**, *38*, 249–256. [CrossRef]
14. Baghdadi, N.; Aubert, M.; Zribi, M. Use of TerraSAR-X Data to Retrieve Soil Moisture over Bare Soil Agricultural Fields. *IEEE Geosci. Remote Sens. Lett.* **2012**, *9*, 512–516. [CrossRef]
15. Zribi, M.; Kotti, F.; Lili-Chabaane, Z.; Baghdadi, N.; Ben Issa, N.; Amri, R.; Amri, B.; Chehbouni, A. Soil texture estimation over a semiarid area using TerraSAR-X radar data. *IEEE Trans. Geosci. Remote Sens. Lett.* **2012**, *9*, 353–357. [CrossRef]
16. Maleki, M.; Amini, J.; Notarnicola, C. Soil roughness retrieval from TerraSar-X data using neural network and fractal method. *Adv. Space Res.* **2019**, *64*, 1117–1129. [CrossRef]
17. Lopez-Martinez, C.; Fabregas, X. Polarimetric SAR speckle noise model. *IEEE Trans. Geosci. Remote Sens.* **2003**, *41*, 2232–2242. [CrossRef]
18. Breunig, F.M.; Galvão, L.S.; Dalagnol, R.; Dauve, C.E.; Parraga, A.; Santi, A.L.; Della Flora, D.P.; Chen, S. Delineation of management zones in agricultural fields using cover-crop biomass estimates from PlanetScope data. *Int. J. Appl. Earth Obs. Geoinf.* **2020**, *85*, 102004. [CrossRef]
19. Georgi, C.; Spengler, D.; Itzerott, S.; Kleinschmit, B. Automatic delineation algorithm for site-specific management zones based on satellite remote sensing data. *Precis. Agric.* **2018**, *19*, 684–707. [CrossRef]
20. Zhao, W.; Qu, Y.; Chen, J.; Yuan, Z. Deeply synergistic optical and SAR time series for crop dynamic monitoring. *Remote Sens. Environ.* **2020**, *247*, 111952. [CrossRef]
21. Han, D.; Wang, P.; Tansey, K.; Liu, J.; Zhang, Y.; Tian, H.; Zhang, S. Integrating an attention-based deep learning framework and the SAFY-V model for winter wheat yield estimation using time series SAR and optical data. *Comput. Electron. Agric.* **2022**, *201*, 107334. [CrossRef]

22. Ouaadi, N.; Jarlan, L.; Le Page, M.; Zribi, M.; Paolini, G.; Hssaine, B.A.; Escorihuela, M.J.; Fanise, P.; Merlin, O.; Baghdadi, N.; et al. Intercomparison of very high-resolution surface soil moisture products over Catalonia (Spain). *Remote Sens. Environ.* **2024**, *309*, 114225. [CrossRef]
23. Breiman, L. Random Forests. *Mach. Learn.* **2001**, *45*, 5–32. [CrossRef]
24. Fieuzal, R.; Baup, F. Estimation of Multi-Frequency, Multi-Incidence and Multi-Polarization Backscattering Coefficients over Bare Agricultural Soil Using Statistical Algorithms. *Appl. Sci.* **2023**, *13*, 4893. [CrossRef]
25. Ouin, A.; Andrieu, E.; Vialatte, A.; Balent, G.; Barbaro, L.; Blanco, J.; Ceschia, E.; Clement, F.; Fauvel, M.; Gallai, N.; et al. Building a shared vision of the future for multifunctional agricultural landscapes. Lessons from a long-term socio-ecological research site in south-western France. *Adv. Ecol. Res.* **2021**, *65*, 57–106.
26. Gaillardet, J.; Braud, I.; Hankard, F.; Anquetin, S.; Bour, O.; Dorfliger, N.; de Dreuzy, J.; Galle, S.; Galy, C.; Gogo, S.; et al. OZCAR: The french network of critical zone observatories. *Vadose Zone J.* **2018**, *17*, 1–24. [CrossRef]
27. Baup, F.; Fieuzal, R.; Marais-Sicre, C.; Dejoux, J.F.; Le Dantec, V.; Mordelet, P.; Claverie, M.; Hagolle, O.; Lopes, A.; Keravec, P.; et al. MCM'10: An experiment for satellite multi-sensors crop monitoring from high to low resolution observations. In Proceedings of the 2012 IEEE International Geoscience and Remote Sensing Symposium, Munich, Germany, 22–27 July 2012; pp. 4849–4852.
28. Breit, H.; Fritz, T.; Balss, U.; Lachaise, M.; Niedermeier, A.; Vonavka, M. TerraSAR-X SAR processing and products geoscience and remote sensing. *IEEE Trans. Geosci. Remote Sens.* **2010**, *48*, 727–740. [CrossRef]
29. Morena, L.C.; James, K.V.; Beck, J. An introduction to the RADARSAT-2 mission. *Can. J. Remote Sens.* **2004**, *30*, 221–234. [CrossRef]
30. Blickensdörfer, L.; Schwieder, M.; Pflugmacher, D.; Nendel, C.; Erasmi, S.; Hostert, P. Mapping of crop types and crop sequences with combined time series of Sentinel-1, Sentinel-2 and Landsat 8 data for Germany. *Remote. Sens. Environ.* **2022**, *269*, 112831. [CrossRef]
31. Dabboor, M.; Xu, J.; Vakalopoulou, M.; Bélair, S.; Powers, J.; Carrera, M.; Sun, L. The RADARSAT Constellation Mission for Soil Moisture Retrieval of Bare Soil by Compact Polarimetry and Random Forest Regression. *Can. J. Remote Sens.* **2024**, *50*, 2356688. [CrossRef]
32. Khabazan, S.; Motagh, M.; Hosseini, M. Evaluation of Radar Backscattering Models IEM, OH, and Dubois using L and C-Bands SAR Data over different vegetation canopy covers and soil depths. *Int. Arch. Photogramm. Remote Sens. Spat. Inf. Sci.* **2013**, *40*, 225–230. [CrossRef]
33. Zeng, J.; Chen, K.-S.; Bi, H.; Zhao, T.; Yang, X. A comprehensive analysis of rough soil surface scattering and emission predicted by AIEM with comparison to numerical simulations and experimental measurements. *IEEE Trans. Geosci. Remote Sens.* **2016**, *55*, 1696–1708. [CrossRef]
34. Slade, B. *Radarsat-2 Product Description*; European Space Agency: Paris, France, 2009.
35. Fritz, T.; Eineder, M.; Mittermayer, J.; Roth, A.; Börner, E.; Breit, H. *TerraSAR-X Ground Segment Basic Product Specification Document*; DLR: London, UK, 2008; p. 103.
36. Ulaby, F.T.; Batlivala, P.P.; Dobson, M.C. Microwave backscatter dependence on surface roughness, soil moisture, and soil texture: Part I—Bare Soil. *IEEE Trans. Geosci. Electron.* **1978**, *16*, 286–295. [CrossRef]

Disclaimer/Publisher's Note: The statements, opinions and data contained in all publications are solely those of the individual author(s) and contributor(s) and not of MDPI and/or the editor(s). MDPI and/or the editor(s) disclaim responsibility for any injury to people or property resulting from any ideas, methods, instructions or products referred to in the content.